A Geant4 Simulation Package for the TASISpec Experimental Detector Setup

Sarmiento, L. G.; Andersson, L. -L.; Rudolph, Dirk

Published in:
Nuclear Instruments & Methods in Physics Research. Section A: Accelerators, Spectrometers, Detectors, and Associated Equipment

DOI:
10.1016/j.nima.2011.11.074

2012

A Geant4 Simulation Package for the TASISpec Experimental Detector Setup

L.G. Sarmiento[*,a,b], L.-L. Andersson[c,1], D. Rudolph[b]

[a] *Universidad Nacional de Colombia, Bogotá D.C. 111321, Colombia*
[b] *Lund University, S-22100 Lund, Sweden*
[c] *University of Liverpool, Oliver Lodge Laboratory, Liverpool L69 7ZE, United Kingdom*

Abstract

The experimental detector setup TASISpec (**TA**SCA in **S**mall **I**mage mode **Spec**troscopy) comprises composite Ge- and highly segmented Si-detectors. The setup is constructed to provide multi-coincidence spectroscopic data between γ-rays, X-rays, conversion electrons, fission fragments, and α-particles for heavy and superheavy elements ($Z \geq 100$).

The full array has been virtually constructed using the Geant4 simulation toolkit. The simulations will not only be used to explore the possibilities of the detector setup itself. More important, however, they will also shed light on the nuclear structure of the heaviest elements. This can be done by comparing the simulated detector response of complex decay modes with the experimental data. Such an iterative or 'self-consistent' way to understand experimental observables will provide more reliability when disentangling the data and deducing experimental decay schemes.

Key words: Decay tagging spectrometer, Alpha, gamma-ray, and conversion electron spectroscopy at recoil separators, Si strip detector, Clover Ge detector, Cluster Ge detector, Geant4
PACS: 23.60+e, 27.80.+w, 29.30.Dn, 29.30.Kv, 29.30.Ep, 07.05.Tp, 29.40.Gx

1. Introduction

The study of heavy ($Z \geq 80$) and superheavy elements ($Z \geq 100$) has proven to be a difficult endeavor for experimental nuclear physics. The small cross-sections are challenged by isotope selection as well as detection efficiency simultaneously. Furthermore, uncertainties in the underlying nuclear shell structure give rise to various theoretical predictions, which are typically in accordance with the experimental findings, which in turn are often based on scarce data.

The superheavy neighborhood is of particular interest because of the possibility to find the so-called "island of stability" [1–4], predicted theoretically to exist in the vicinity of the still experimentally unknown magic numbers for regimes of protons and neutrons at the upper edge of the chart of nuclides.

In order to sail to *the island*, TASCA, a gas-filled recoil separator located at the GSI Helmholtzzentrum für Schwerionenforschung GmbH in Darmstadt, Germany, was developed [5]. Its purpose is to separate the precious superheavy nuclei from the huge experimental background of particles produced in the nuclear reaction. When TASCA is operated in *Small Image Mode* (Sec. 1.1) it allows the placement of a high-resolution, highly segmented Si- and Ge- detector array around its compact focal plane [6].

To aid the data analysis and to explore the full capacities of the current setup, TASISpec has been constructed virtually using the Geant4 toolkit [7]. This allows predictions of the detector performance of future experiments as well as assess results from the data analysis. In addition, the simulation can guide in decisions on possible upgrades for the detection system in the future.

1.1. TASCA in Small Image mode (TASISpec)

The TASCA gas-filled recoil separator uses a combination of one bending dipole magnet and two focusing quadrupole magnets allowing for two different ion optical focusing modes. These are the *High Transmission Mode* (HTM) and the *Small Image Mode* (SIM) [5]. When operated in SIM the transmission is typically 35% for evaporation residues in reactions aimed to produce heavy or superheavy elements [8]. The SIM has the advantage of a very small focal plane image. The residues end up in a slightly elliptical image of about 3 cm in

[*] Corresponding author
Email address: lgsarmientop@unal.edu.co (L.G. Sarmiento)

[1] Present address: Helmholtz Intitute Mainz, D-55099 Mainz, Germany

diameter [5], thus allowing high-resolution Ge- and Si-detectors to be placed around it in an very compact way.

The TASISpec detection setup utilizes the TASCA SIM focal mode and combines double-sided (DSSSD) and single-sided (SSSSD) Si-strip detectors with composite Ge-detectors [6]. The underlying philosophy is to provide a compact inner Si-detector cube, which should be as transparent as possible to low-energy γ- or X-rays.

More details regarding the setup and its commissioning experiments can be found in Ref. [6].

2. Modeling TASISpec using GEANT4

The geometry of TASISpec includes both active and inactive elements. Both of these have been included in the Geant4 detector reconstruction to achieve a realistic scenario and reproduce the experimental situation in great detail. The complete simulated setup includes the following active elements; one DSSSD, four SSSSD, two *VEGA* Clover detectors [9], two *EUROGAM* Clover detectors [10] and one *EUROBALL* Cluster detector [11, 12]. Inactive elements such as the beam transfer tube, preamplifiers holder, vacuum chamber, printed circuit boards (PCB) and the Ge-detector's aluminum casings are also included.

2.1. Si-detectors

The incoming residual ions from the TASCA separator impinge into a 57.8 mm x 57.8 mm, 32x32 strip DSSSD, 0.52 mm thick. The active elements in this detector, due to practical reasons, are simulated to include a total of 1024 pixels rather than the 64 individual p- and n-side perpendicular strips.

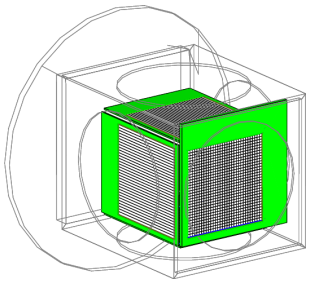

Figure 1: The highly segmented Si-array as coded in the simulation. The vacuum chamber is drawn by continuous lines. Note the circular regions on each of five sides of the cube-like cap. These indicate regions with thinner chamber walls to minimize attenuation of the X- and γ-rays. The PCBs onto which the silicon detector are mounted are depicted and the corresponding pixels (strips) of the DSSSD (SSSSD) can also be seen. See text for details.

Four 32-fold segmented SSSSD with active areas of 59.5 mm x 59.5 mm and 0.97 mm thick form, in conjunction with the implantation DSSSD, a cube-like structure with a total of $1024 + 4 \cdot 32 = 1152$ Si-detector units. One side of the cube is left open for the incoming particles from the separator. The DSSSD acts as an implantation and charged-particle decay detector from where the position and energy of the implants are obtained. The SSSSDs aim at detecting conversion electrons, α-particles which escape full absorption in the DSSSD, and fission fragments. This configuration, seen in Fig. 1 (ions entering from the back) allows for the study of the full decay chains using multiple-coincidences between the different detector channels when used in close conjunction with composite Ge-detectors.

To further detail the simulation and hence its prediction accuracy, the TASISpec transfer tube, the holders of the preamplifiers as well as a very detailed geometry of the vacuum chamber surrounding the Si detectors were also implemented. The chamber was modeled as five 3.0 mm thick aluminum walls; each of the walls has a circular area of 85 mm in diameter where the wall thickness is only 1.5 mm. This feature aims to reduce the attenuation of low-energy X- and γ-rays. PCBs, and the front, and ohmic SiO_2 dead layers for the Si-detectors were included. Cables and connectors were however not included in the simulation.

2.2. The Ge-detectors

Along with the charged-particle emission from the decay, the X- and γ- rays constitute often decisive parts in the decay chains. Three kinds of Ge-detectors are used closely packed around the vacuum chamber:

2.2.1. Clover detectors

Both VEGA and EUROGAM kind of Clover detectors consist of four closely packed coaxial Ge diodes [9, 10]. Each originally cylindrical crystal has a length l and a diameter d and it is shaped in such fashion that the front face has a quasi-squared section by beveling two adjacent faces with a given angle θ. The remaining two faces parallel to the crystal axis are tapered along its whole length [10]. The Clover detectors are contained in vacuum protected by an aluminum casing of thickness th. The dimensions of both Clover detectors are listed in Table 1. A VEGA Clover is shown in Fig. 2.

The cylindrical high voltage (HV) hollowing in the rear part of the crystals was also included in the simulation of the Clover crystals. In the case of the EUROGAM crystals the same 15 mm Ge thickness from the HV hole to the crystal end cap from the VEGA Clover was kept. The hollowing diameter was assumed

Type	l	d	θ(°)	th	l_{HV}	d_{HV}
I	140.0	70.0	15.0	2.0	125.0	10.0
II	70.0	50.0	7.1	1.5	55.0	7.1

Table 1: Basic dimensions of the different Clover detector used the simulated TASISpec. For both VEGA (I) and EUROGAM (II) detectors. All lengths are given in mm. See text for details.

to be scaled down by the same ratio as the diameters of the two crystals. The EUROGAM crystals as programmed in Geant4 were reduced to 89.12(4)% of the volume of a cylinder according to the *GetVolume()* Monte Carlo method from Geant4. A difference of about 0.1% to the reduction reported value for the shaping of such crystals [10]. Each one of the Clover detectors is placed behind one of the four SSSSD as illustrated in Fig. 4. Since BGO suppression shielding is not used in TASISpec, it was not included in the simulation. Cryostats are not included in the simulation either although in the experimental setup they are physically present.

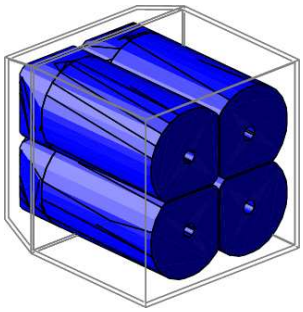

Figure 2: One of the two EUROGAM Clovers programmed in Geant4. Four individual crystals are shown and the aluminum casing is illustrated with continuous lines. Note the internal HV fingers and the close packing achieved. See text for details.

2.2.2. *Cluster detector*

The EUROBALL Cluster detector consists of seven closely packed hexagonal encapsulated Ge-detectors [12]. Like in the Clover case, no BGO shielding was used and the cryostat was not included in the virtual geometry either. Each crystal is 70 mm in diameter and 78 mm long before shaping with a 53 mm deep HV finger of 6 mm in diameter. The close packing of the seven crystals while keeping a high percentage of the crystal (91.1%) is achieved thanks to the semi-hexaconical shaping procedure [13] displayed in Fig. 3. The difference in volume after shaping between the virtual and the actual crystal is less than 2%. Each crystal is encapsulated in a 0.7 mm thick Al case. The

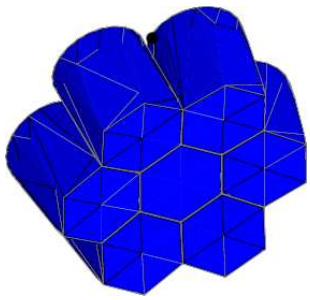

Figure 3: Visualization of one the Ge Cluster detector. See text for details.

seven crystals composing the complete Cluster detector are inside another Al canister with a 1.5 mm thick wall assumed in accordance to the VEGA Clover detectors. The Cluster is placed behind the DSSSD where the maximum angular detection coverage for the implanted nuclei can be achieved. Figure 4 visualizes the complete coded setup where top and left are VEGA Clovers and bottom and right are EUROGAM Clovers. In the background the EUROBALL Cluster from Fig. 3 can be seen. In the foreground the transfer tube and preamplifier holding structures are indicated by continuous circular lines.

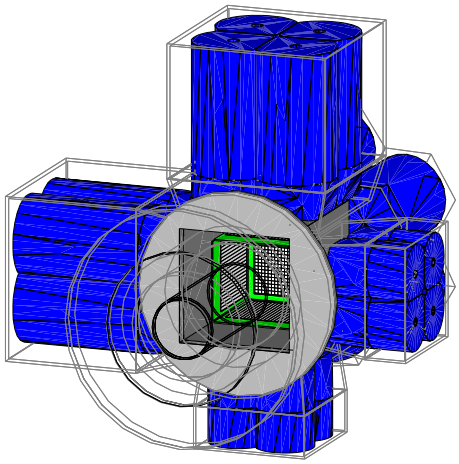

Figure 4: The full virtual TASISpec setup. All the Ge-crystals are depicted solid and its casing suggested by straight lines. The vacuum chamber and transfer tube are provided by circular continuous lines. The ions enter the setup from the front side, through the transfer tube, and into the cube-like Si-detector assembly from Fig. 1.

3. Software handling of the simulations

The detector signals from the experiment are being handled using an offline sort code to account for features such as scattering between detector segments and

different gating and selection methods. The simulated single hits are treated the same way for a consistent comparison. This Section deals with the comparisons between experiment and simulation to explore the overall reliability of the simulations.

Figures and numbers presented below use the Geant4 version 9.4 (December 2010). The simulations using radioactive sources are based on the Geant4 Radioactive Decay Module (GRDM) built into the Geant4 packages and utilizes the empirical data from the most recent RadioactiveDecay3.3 and PhotonEvaporation2.1 data files available to date. The Livermore physics list of low-energy electromagnetic processes was chosen. If not stated otherwise the simulated results using the radioactive sources involve 10 million decaying nuclei each.

3.1. The Ge-detector efficiency

The efficiency of the Germanium detectors using the TASISpec setup has been compared in detail with the experimental measurements. This can be done in two ways: *(i)* The general shape of the efficiency curve, i.e. the relative efficiencies, can be compared using a point-like calibration source placed on a source holder. *(ii)* The absolute efficiency can be compared by means of well known α - γ correlations originating from the decay of evaporation residues being implanted in the detector.

To compare the relative efficiencies the experiment utilizes radioactive sources placed on a source holder. The holder consists of a solid rod made of polyethylene. This rod is inserted into the detector array through the transfer tube which can be seen at the left-hand side of Fig. 4. The top of the holder – onto which the radioactive source is placed – is positioned opposite the DSSSD, some 55 mm away from the front face of the wafer.

Two radioactive sources were used in both experiment and simulations: ^{152}Eu and ^{133}Ba, chosen to cover a large range of γ-ray energies. For the simulations the rod was reconstructed in Geant4 and placed into the setup to mimic the real life scenario where it actually shadows some of the Ge-crystals, mainly those placed furthest from the DSSSD. In the simulation, as well as in the experiment, the Ge-signals have a 20 keV software threshold. In addition the simulations have a detection probability,

$$P_\gamma = \tan\Big(E_\gamma[\text{in keV}] - 10\Big), \qquad (1)$$

for γ-rays between 20 keV and 55 keV, defined to mimic the charge collection process to address the fact that charge collection is strongly energy-dependent for low γ-ray energies.

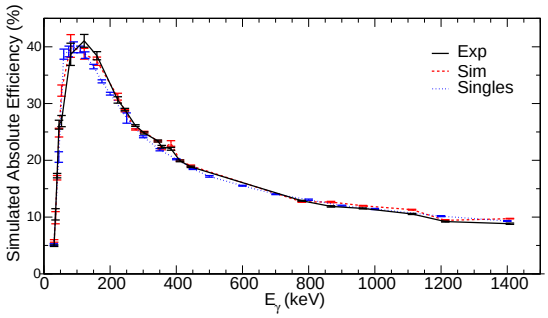

Figure 5: The Ge-detector's total detection efficiency as a function of γ-ray energy. The solid curve shows experimental results using ^{133}Ba and ^{152}Eu standard sources placed on the radioactive source holder, the dashed curve shows the corresponding simulated results. The dotted curve shows simulated results using an "ideal" calibration source which emits only one single γ-ray per event. See text for discussion and details.

Figure 5 shows the comparison between simulations and experiment using two radioactive sources (^{133}Ba and ^{152}Eu) placed – one at a time – on the source holder. Only single γ-rays detected in the Ge-crystals are included in this plot, i.e. no software reconstruction of Compton scattered γ-rays (add-back) are taken into account.

The experimental results involve only information about relative intensities. The normalization between the two radioactive sources are based on the yields of the 344.3 keV $\left(^{133}\text{Ba}\right)$ and the 356.0 keV $\left(^{152}\text{Eu}\right)$ transitions in the simulations. Over the region of interest the experimental curve (solid) is normalized to the simulated one (dashed) to compare relative intensities only.

It should be noted that the simulations differ from the experimental detection process in one specific aspect. While the simulations are restricted to one single nucleus to decay at a time, a radioactive source may have many nuclei decaying simultaneously. Such a scenario results in an increased probability of several individual γ-rays – for example the 302.9 keV and 81.0 keV transitions from ^{133}Ba – to enter one crystal and be detected as one single γ-ray at 383.4 keV. This event would give an increase in efficiency for the 383.4 keV transition and a decrease in detected intensity for the two individual γ-rays. This trend can also be seen in both the simulated and the experimental plots presented in Fig. 5 where the efficiency curves increase slightly at 383.4 keV transition and hence decreases at 302.9 keV and 81.0 keV. However, while the simulations accept such an event as a single detected γ-ray, the electronics used in the experiment may reject this event due to pile-up in the detector. Pile-up rejection in the current experimental electronics

scheme is implemented if one or more signals are detected in the crystal during the trigger gate opened by the first signal, i.e. within 10 μs.

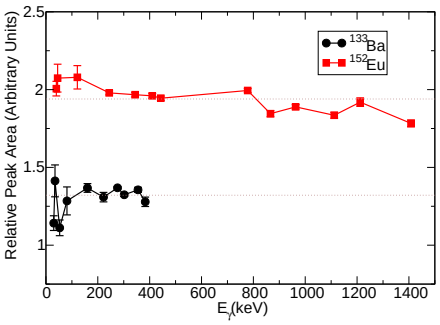

Figure 6: The ratio between the integral of the peaks in the experiment and simulation. A constant difference is expected for a perfect fit. See text for details.

To avoid "natural" summing fluctuations originating from two γ-rays from the same nucleus entering the same crystal it is possible to compare only the area of each peak separately. This is done in Fig. 6. Here the background subtracted area under the graph fitted with the same background region for the simulated and experimental spectrum is compared as a function of γ-ray energy. The y-axis gives the fraction of the two areas in arbitrary units. For a perfect simulation the fraction should remain constant for all transitions. As can be seen the largest discrepencies appear at low energies where the charge collection process is much more difficult to replicate.

For comparison Fig. 5 also includes the results for a simulated "ideal" calibration source. The source is placed on the holder and decays from the ground state in the mother nucleus into one excited state of the daughter nucleus. This state then decays immediately via a pure γ-ray transition, i.e. no internal conversion is present and no "false" γ-ray summing can occur. The excited state in the daughter nucleus has been given different energies to produce the different points on the curve. Each data point is simulated for 150 000 events.

3.1.1. Reconstructing Compton scattered γ-rays

The offline software handling of scattered γ-rays, the so-called add-back correction, is described in this section. The correction can be either what is here referred to as *internal* add-back, between crystals in the same detector [11]. Such method can be extended to the so-called *cross-detector* add-back, between crystals in two different detectors. The latter are naturally more likely for crystals placed next to each other in the detector geometry (see Fig. 7). At present, in the reconstruction, γ-rays are allowed to scatter once, meaning at maximum two crystals are involved in the detection.

To optimize the add-back for true Compton-scattered events and minimize the risk of adding together two promptly emitted γ-rays from the source, the energy deposited in the two crystals is limited by the angle between them and hence the relative energies. The Compton scattering formula can be re-written as

$$\frac{E - E'}{E \cdot E'} = \frac{1 - \cos\theta}{m_e c^2}, \tag{2}$$

where E is the initial energy and E' is the remaining energy of the γ-ray after scattering. Figure 7 illustrates an example of the process. The trajectories show θ_{min} and θ_{max} referring to the extreme scattering angles.

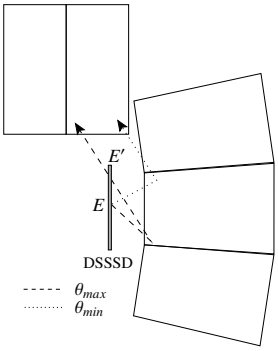

Figure 7: An example of the Compton cross-detector scattering process. A schematic drawing of a cross-section of two of the involved Ge-detectors in the full detector array. Two crystals in the top Clover are shown and also three crystals of the Cluster. The example shows the scattering of a γ-ray with energy E starting in the DSSSD entering the center crystal in the Cluster detector and then scattering into one of the top clover crystals. The minimum, θ_{min}, and maximum, θ_{max} scattering angles involved are indicated.

Since the scattering involves a minimum, θ_{min}, and maximum, θ_{max} angle, the restricted scattering angle in Eq. 2 gives limitations on the ratio of the involved energies, E' and E. These limitations are implemented in the offline analysis by means of two dimensional gates.

While the internal add-back allows the efficiency to increase for the high energy γ-rays, the cross detector add-back mainly decreases the amount of unwanted background. In Fig. 8 the effect of the internal and cross-detector add-backs are illustrated using the $11/2^- \rightarrow 9/2^+ \rightarrow 7/2^+$, 221 keV-58 keV cascade in ^{253}No [14]. The 58 keV transition, which is highly converted, is in coincidence with the intense 221 keV transition [14]. The figure shows the detected γ-ray spectrum in coincidence with the 58 keV line. In the spectrum in the top panel no add-back is included. The

true coincidence is clearly observed at 221 keV but the peak at 163 keV originates from scattered 221 keV γ-rays, when depositing 58 keV in one Ge-crystal and the remaining 221-58=163 keV in a different crystal. By applying the internal add-back (middle panel) the intensity of this "false" coincidence is substantially reduced. When applying both internal and cross-detector add-back (bottom panel) the intensity is again slightly reduced together with the background, while the intensity of the true coincidence at 221 keV also increases slightly.

Figure 9 shows the simulated efficiency curves for singles, internal add-back and a combination of internal and cross-detector add-back using the decay of the "ideal" nucleus described in Sec. 3.1. The nuclei are here moving with 35(5) MeV kinetic energy – typical value for recoils in TASCA – and are implanted into the DSSSD before they decay. It should also be noted that the simulations here follow a realistic implantation profile, see Fig. 10, for completeness. However, it has been shown that the implantation profile is of minor importance in the TASISpec setup as within errors one ends up with the same efficiencies no matter the distribution of simulated nuclei in the DSSSD. To get a feel for how accurately the simulations reproduce the behavior of the real setup, three experimental efficiencies are included from α - γ correlations of implanted nuclei. These are seen in 9. In general the agreement is good although the higher energies are slightly overestimated in the simulations.

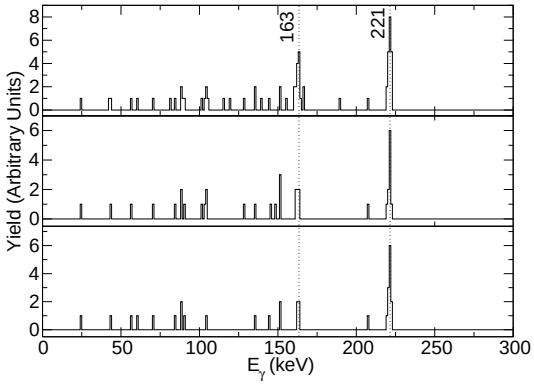

Figure 8: The γ-ray experimentally detected in coincidence with the 58 keV transition in ^{253}No. The upper panel shows the spectrum using no add-back, the middle panel includes internal add-back and the bottom panel includes both internal and cross-detector add-back. See text for details.

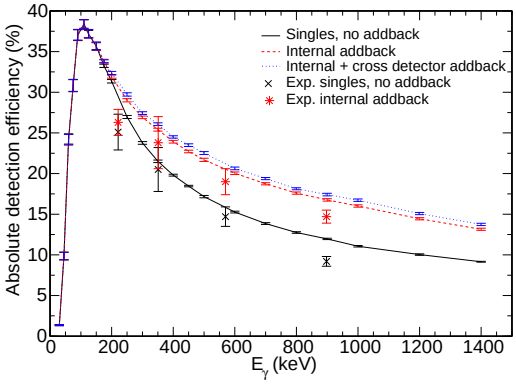

Figure 9: An implanted nucleus is allowed to decay to its ground-state via one single γ-ray. Each energy is simulated for 150 000 decays. The resulting efficiency curves are shown when using no add-back, internal add-back, and internal plus cross-detector add-back. In addition three experimental points are included. These are originating from α - γ-correlations. Each experimental point is included with both no add-back and internal add-back accounted for.

3.2. The Si detection efficiency

The Si detectors have been reported in Ref. [6] to have the following detection efficiencies for α-particles: The DSSSD has 50% efficiency for fully absorbed particles, and the four box detectors together have 30(2)% for α-particles which escape full detection in the DSSSD. This results in a total α-detection efficiency of 80(2)%. Furthermore, it is assumed that 100% of the implanted ions are detected in the DSSSD. These numbers are based on a heavy-ion reaction from the experiment with an implantation profile in the DSSSD detector according to panel A in Fig. 10.

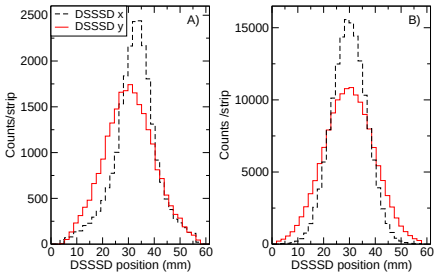

Figure 10: In panel A the hit pattern in the DSSSD from an experiment is illustrated. The hits are gated on the 8.0 MeV α-particle from ^{253}No. Note that no background subtraction has been done. Panel B shows the corresponding hit pattern from the α-particles in the simulations which intend to mimic the experimental profile, this pattern contain no background counts. The x-axes give the size of the DSSSD in mm.

When looking at the Si detectors using the Geant4

simulation code it is assumed that the impinging ions have the same 35(5) MeV kinetic energy as in the experimental situation. The implantation profile can be seen in panel B in Fig. 10. From this it is found that 98% of the implanted ions are detected in the DSSSD and that they are implanted into the Si detector at a depth of 6.8(1) μm which is typical for a heavy ion with $Z \approx 100$ and $A \approx 250 - 260$. If an ion implanted at this depth then decays by emitting an 8.0 MeV α-particle the efficiency of the DSSSD to fully absorb the energy of the α-particle is 55%, while 31% of the α-particles will be ejected out of the DSSSD to enter and deposit some energy in either of the four Si-box detectors. The remaining 14% will deposit some energy in the DSSSD before escaping out through the open face of the Si-cube. This means that the simulations give a total α-detection efficiency of 86%, slightly higher than the experimental estimation from Ref. [6].

The detection efficiency in the different Si detectors will, of course, depend on the implantation depth. For example if assuming half of the kinetic energy compared to the case above for the impinging ion, the implantation depth will be 4.0(1) μm which yields 52% of 8.0 MeV α-particles detected in the DSSSD and 34% in the box detectors.

4. Summary and Outlook

The simulation toolkit Geant4 was mainly aimed for High Energy Physics simulations. It is nonetheless in continuous development and with time its usage has spread widely among other areas.

At present it is not possible to simulate the radioactive decay of superheavy elements using the GRDM in a natural way, since there is a $Z \leq 100$ restriction along the source code. However, according to the 'Planned developments for 2011' [15] such decays will be coded for the first time into the Geant4 source code, opening up for yet another field to be able to utilize the Geant4 simulations.

In this paper the usage of a very detailed Geant4 geometry was presented. This together with a careful Physics List choice can shed new light on the superheavy elements research. It is not only because it is possible to test the experimental data corrections such as add-back routines and charged-particle and γ-ray efficiency but because it also provides an excellent testing scenario for new gating and triggering possibilities, providing us with a more profound way to explore the scarce experimental data.

The TASISpec detection setup is being continuously improved and developed. The corresponding Geant4 code thus naturally has to continue its evolution to remain accurate and provide simulations which are true to reality. Such improvements sometimes involve minor adjustments like the diameter of the transfer tube, the space that the evaporation residues have to travel through in order to be implanted into the DSSSD. Nevertheless, some modifications are more substantial like the upgrade from SSSSD to DSSSD detectors in the box section, or the inclusion of NaI scintillation detectors to suppress some of the Compton scattering between the Ge-detectors. Furthermore, some modifications even need to be continuously adjustable to suit different experiments like for example the thickness of the implantation detector.

The TASISpec simulation package has also been modified to suit the environment behind the SHIPTRAP [16] at GSI. Some of the TASISpec detectors have been used here in the so-called TRAPSpec configuration for a commissioning experiment [17].

Acknowledgments

The authors would like to thank the TASISpec and TASCA collaborations for fruitful discussions and support. We also thank the GSI support staff for invaluable help during the setup and data collection during the experiments.

L.G. Sarmiento would like to thank COLCIENCIAS for funding through the program *Doctorados Nacionales* and L.-L. Andersson would like to thank the Royal Physiographic Society in Lund (Hellmuth Hertz foundation) and the Swedish Research Council for financial support.

References

[1] S. G. Nilsson *et al.*, Nucl. Phys. A **115**, 545 (1968).
[2] E. D. Fiset and J. R. Nix, Nucl. Phys. A **193**, 647 (1972).
[3] Yu. Ts. Oganissian, Phys. Atom. Nucl., **63**, 1315 (2000).
[4] M. A. Stoyer, Nature **442**, 876 (2006).
[5] A. Semchenkov *et al.*, Nucl. Instrum. Meth. Phys. Res. B **266**, 4153 (2008).
[6] L.-L. Andersson *et al.*, Nucl. Instrum. Meth. A **622**, 164 (2010).
[7] S. Agostinelli *et al.*, Nucl. Instrum. Meth. A **506**, 250 (2003).
[8] J. M. Gates *et al.*, Phys. Rev. C **83**, 054618 (2011).
[9] J. Gerl, H. Grawe, E. Roeckl, H. J. Wollersheim, VEGA a proposal for Versatile and Efficient Gamma-detectors, GSI Darmstadt, Report, 1998.
[10] G. Duchêne *et al.*, Nucl. Instrum. Meth. A **432**, 90 (1999).
[11] J. Eberth *et al.*, Nucl. Instrum. Meth. A **369**, 135 (1996).
[12] J. Simpson, Z. Phys. A **358**, 139 (1997).
[13] H.G. Thomas, Entwicklung eines Ge-CLUSTER-Detektors für das Gamma-Spektrometer EUROBALL, Verlag Dr. Koester, Berlin, ISBN3-89574-113-2.
[14] `http://www.nndc.bnl.gov/ensdf/`. Last access October 2011.

[15] http://geant4.cern.ch/support/planned_features.shtml. Last access October 2011.
[16] J.B. Neumayr *et al.*, Nucl. Instr. Meth. B **244**, 489 (2006).
[17] D. Rudolph *et al.*, GSI Scientific Report 2009, p. 177, GSI Report 2010-1.